Electronic Supplementary Material (ESI) for Physical Chemistry Chemical Physics.

Supplementary Information of "Formation of α-helical and β-sheet Structures in Membrane-bound human IAPP Monomer and the Resulting Membrane Deformation"

Qin Qiao[1,2*], Guanghong Wei[3], Demin Yao[1,2], Zhijian Song[1,2]

[1]Digital Medical Research Center, School of Basic Medical Sciences, Fudan University, Shanghai 200032, China

[2]Shanghai Key Laboratory of Medical Imaging Computing and Computer Assisted Intervention, Shanghai 200032, China

[3]Department of Physics, State Key Laboratory of Surface Physics, Key Laboratory for Computational Physical Science (Ministry of Education), Fudan University, Shanghai 200438, China

Email: qinqiao@fudan.edu.cn

1. Formation of α-helical structures in the hIAPP N-terminal region and the resulting membrane deformation.

Besides the one of inserted α-helical hIAPP discussed in the main-text (labelled as α-1), there are another two trajectories, in which hIAPP monomer also forms transient α-helical structures at the N-terminus. We will discuss the details of the hIAPP conformational dynamics and the resulting membrane deformation of these two α-helical-rich trajectories as follows.

In one of the α-helical trajectories (labelled as α-2), hIAPP becomes more expanded upon adsorbing on the membrane, as shown in the Fig. S2(a). The hIAPP radius of gyration R_g increases from 9.4 Å to 10 Å, and the radius of gyration about z-axis R_g^z increases from 7.4 Å to 8.7 Å. The N-terminal segment T4-R11, as well as segment F23-I26, form α-helices transiently on the membrane surface, as shown in Fig. S2(b). The α-helical-rich segment A5-Q10 inserts into the membrane tail groups at around 1400 ns, and its C7-Q10 α-helices partially deform during this transient insertion. Meanwhile, the hydrophobic segment F15-V17 forms substantial contacts with membrane tail groups from 300 ns, as shown in the Fig. S2(c). The 2-d free energy projection on the contact number with head and tail groups is shown in Fig. S2(d), and the representative conformations are shown around with arrows directed.

In another α-helical trajectory (labelled as α-3), the hIAPP R_g and R_g^z increase from 9.1 Å to 11 Å and from 7.2 Å to 10 Å respectively, as shown in Fig. S3(a). Two segments at the N-terminal region, T4-C7 and A12-S19, adopt transient α-helical structures on the membrane surface. Meanwhile, the amphiphilic segment N3-T6 forms contact with lipid tail groups transiently with the hydrophobic side-chain of A5 inserting into the membrane head-tail interface. The 2-d free energy projection on the hIAPP contact number with head and tail groups is shown in Fig. S3(d), with the representative conformations shown around.

The membrane thinning and bending caused in the trajectories α-2 and α-3 are larger than those in the inserted α-helical trajectory α-1, as shown in Fig. S5(a, b). This further supports the conclusion in the main-text that the adhesion of hIAPP, rather than its insertion, causes membrane bending. Meanwhile, the tail disordering effects by the α-helical monomers are weak and within the standard deviation of pure POPG bilayer, as shown in Fig. S5(c-f). Moreover, the α-helical structures on the surface (trajectories α-2 and α-3) has small coherence length of membrane thinning ($\xi_{\alpha\text{-}2}$~6.7 Å, $\xi_{\alpha\text{-}3}$~6.7 Å, see the inset of Fig. S5(a)), and the size distribution of membrane hydrophobic defects, as well as the APL are also less perturbed than those of the inserted hIAPP α-1 (see Fig. S5(g, h)). The representative conformations and the POPG lipid molecules of the highest contact probability with hIAPP are shown in Fig. S5(i) for these α-helical-rich trajectories.

In the α-2 and α-3 trajectories, the insertion of hIAPP is also synchronized with the formation of large hydrophobic defects, as shown in Fig. S6(b, c). Meanwhile, the inverse correlation between insertion and membrane bending was observed in trajectory α-3 (see Fig. S6(c)) which is the same as the trajectories discussed in the main-text. On the other hand, the hIAPP insertion and membrane bending is not correlated in trajectory α-2 however (see Fig. S6(b)). The reason for this de-synchronization is probably that the insertion of hydrophobic residues F15-V17 is away from the location of minimal membrane thickness.

Last but not least, the binding of α-helical hIAPP monomers slows down the lipid rotational dynamics. The relaxation time-scales of both head and tail groups (τ_H and τ_T) increase at least one order of magnitude compared to those of pure POPG bilayer, as shown in Fig. S7. The slow-down of head group rotation is most significant in α-2 trajectory, where the slowest τ_H is around 150 ns. In contrast, the slowest τ_H in trajectories α-1 and α-3 are around 20 ns. Interestingly, we found that the slow-down effect caused by R11 is stronger than that by K1. As shown in Fig. S8, R11 is in tight contact with the glycerol and phosphate groups in the α-2, coil, and β-sheet trajectories, where the slowest τ_H is at the order of

10^2 ns. In comparison, in the α-1 and α-3 trajectories where τ_H is around 20 ns, K1, rather than R11, forms tight contacts with the glycerol and phosphate groups. For the tail groups, the relaxation time-scales τ_T are around 10^2 ns for all the α-helical-rich trajectories.

2. The position of each hIAPP residue relative to the POPG membrane.

To illustrate the position of hIAPP relative to POPG in detail, we first calculated the average contact number between hIAPP and POPG tail groups, in the resolution of residues for hIAPP and carbons for lipid tail groups. As shown in Fig. S9, we found that the positively-charged residues (K1 and R11) as well as polar residues (N3, T6, and Y37) form large number of contacts with the 1st carbon closest to the head groups in the aliphatic tail groups. The contact numbers of K1 and R11 reduce with the increase of carbon ID, indicating that these two positively-charged residues are located at the head-tail interface. The hydrophobic residues, i.e. A5, A8, and F23, have substantial contact number with the 14th tail carbons at the lipid end, indicating their deep insertion. Interestingly, the polar residues T6 and Y37 also form notable contacts with carbons deep inside.

We also calculated the time-evolved number of contacts between hIAPP and POPG in each trajectory, summarized in Fig. S10. We divided the POPG lipid into three regions: the head group, the tail segment 1 (Tail 1) from the 1st carbon to the 7th carbon, and the tail segment 2 (Tail 2) from the 8th carbon to the end, which correspond to the adsorption, shallow insertion, and deep insertion, respectively. As shown in Fig. S10, the positively-charged residues K1 and R11 form large contact numbers with POPG head groups in all the trajectories. We observed the amphiphilic N-terminal residues (A5, T6, A8, and T9) form large number of contacts with the deep Tail-2 segment in the trajectories of coiled and α-helical hIAPP structures (Coiled and α-1). Meanwhile, the hydrophobic residues L16 and F23 also insert deep and form contacts with the Tail-2 segment. In the trajectories of α-helical (α-3) and β-hairpin (β) structures on the membrane surface, however, the polar residue Y37 transiently inserts into the Tail-2 segment, while the N-terminal residues are at the shallow Tail-1 segment.

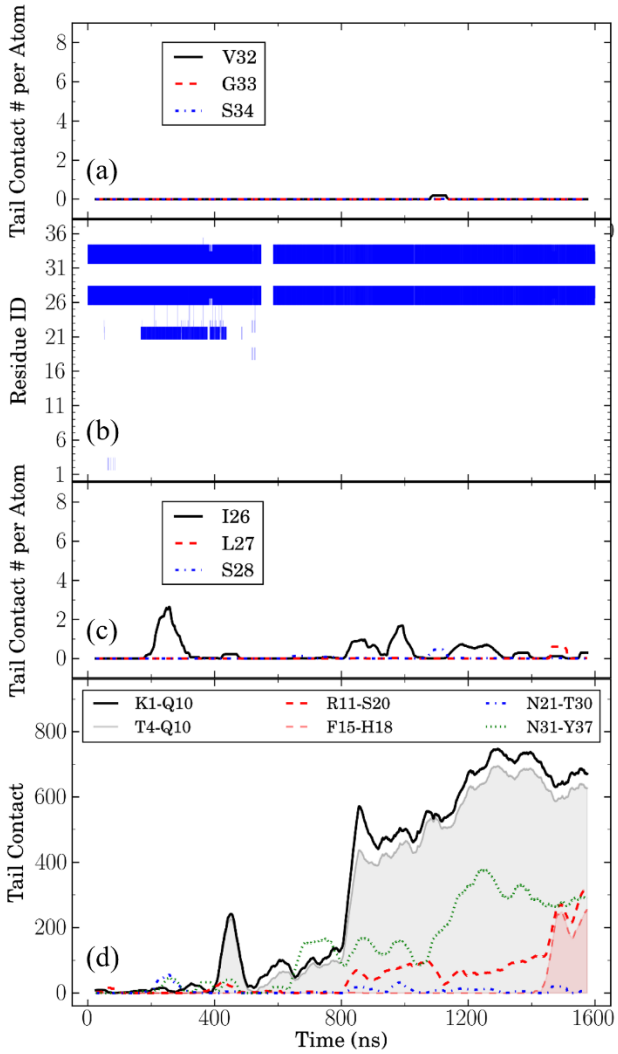

Fig. S1. (a-c) Formation of β-sheet structures at C-terminal region in the trajectory shown in main-text Fig. 3 (labelled as α-1), in which the α-helix at N-terminal region inserts into the POPG head-tail interface. (a) Time evolution of residue-based contact number between β-sheet segment V32-S34 and lipid tail groups. (b) Time evolution of β-sheet secondary structures. (c) Time evolution of residue-based contact number between β-sheet segment I26-S28 and lipid tail groups. (d) Time evolution of contact number between hIAPP segments and lipid tail groups: segment K1-Q10 (black line); segment T4-Q10 (gray line); segment R11-S20 (red line); segment F15 -H18 (light red line); segment N21-T30 (blue line); segment N31-Y37 (green line). The lines in (a), (c), and (d) were smoothed via a 50-ns sliding window.

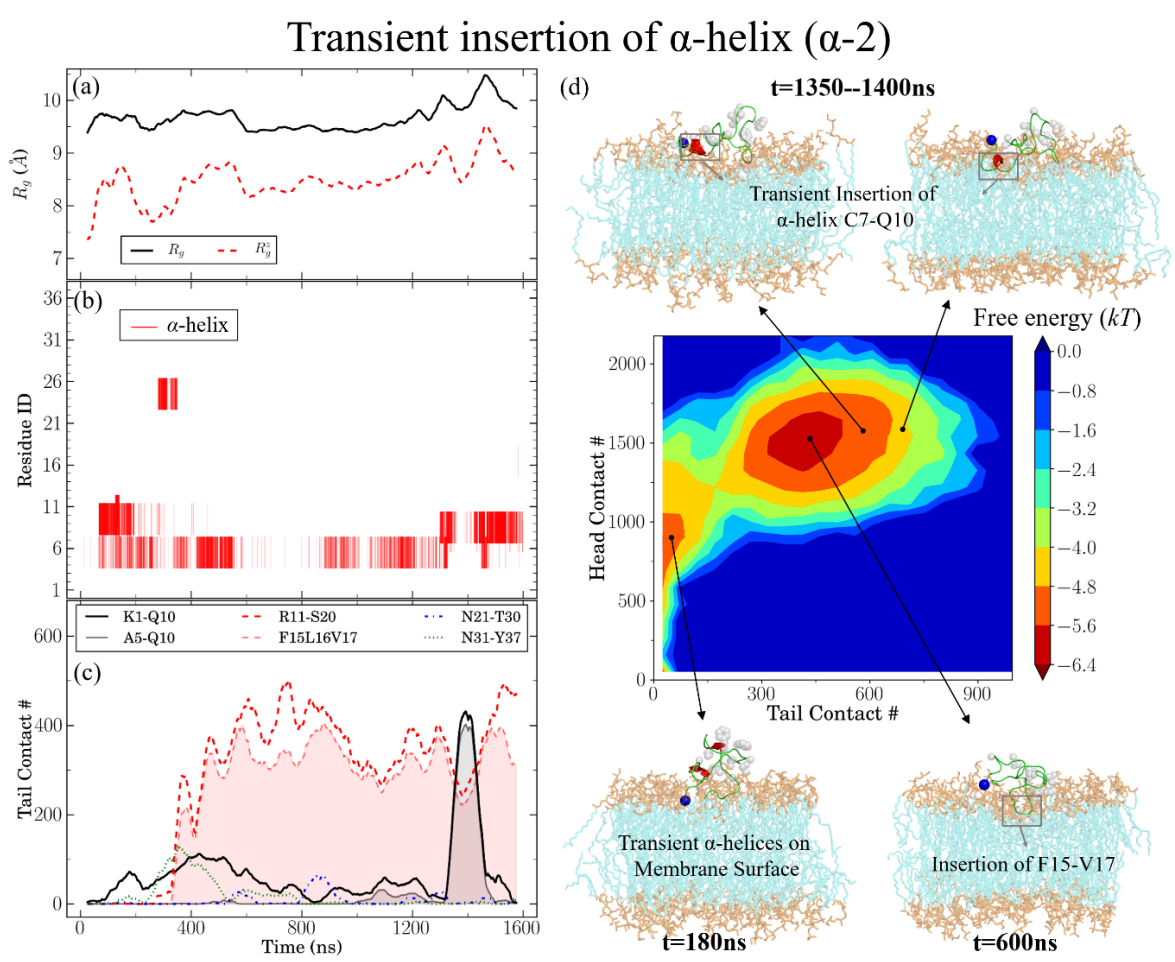

Fig. S2. Conformational dynamics of transient α-helical formation upon binding to POPG membrane (labelled as α-2). (a) Time evolution of hIAPP radius of gyration about the principal axis R_g (black line) and z-axis R_g^z (red line). (b) Time evolution of α-helix secondary structure. (c) Time evolution of contact number between hIAPP segments and lipid tail groups: segment K1-Q10 (dark black line); segment A5-Q10 (light black line); segment R11-S20 (dark red line); residues F15L16V17 (light red line); segment N21-T30 (blue line); segment N31-Y37 (green line). The lines in (a) and (c) were smoothed via a 50-ns sliding window. (d) Free energy landscape is projected onto hIAPP contact number with lipid tail groups (x-axis) and head groups (y-axis), indicating the hIAPP insertion depth. Representative conformations of free energy minima are shown around with arrows directed. In each conformation, hIAPP is shown in cartoon representation, with α-helix in red, β-sheet in yellow, and coil in green. The side-chains of hydrophobic residues are shown in gray spheres. The Cα atom of residue K1 is shown in blue sphere, indicating the N-terminus of hIAPP. POPG lipid bilayer is shown in stick representation, with the head groups in orange, and tail groups in cyan.

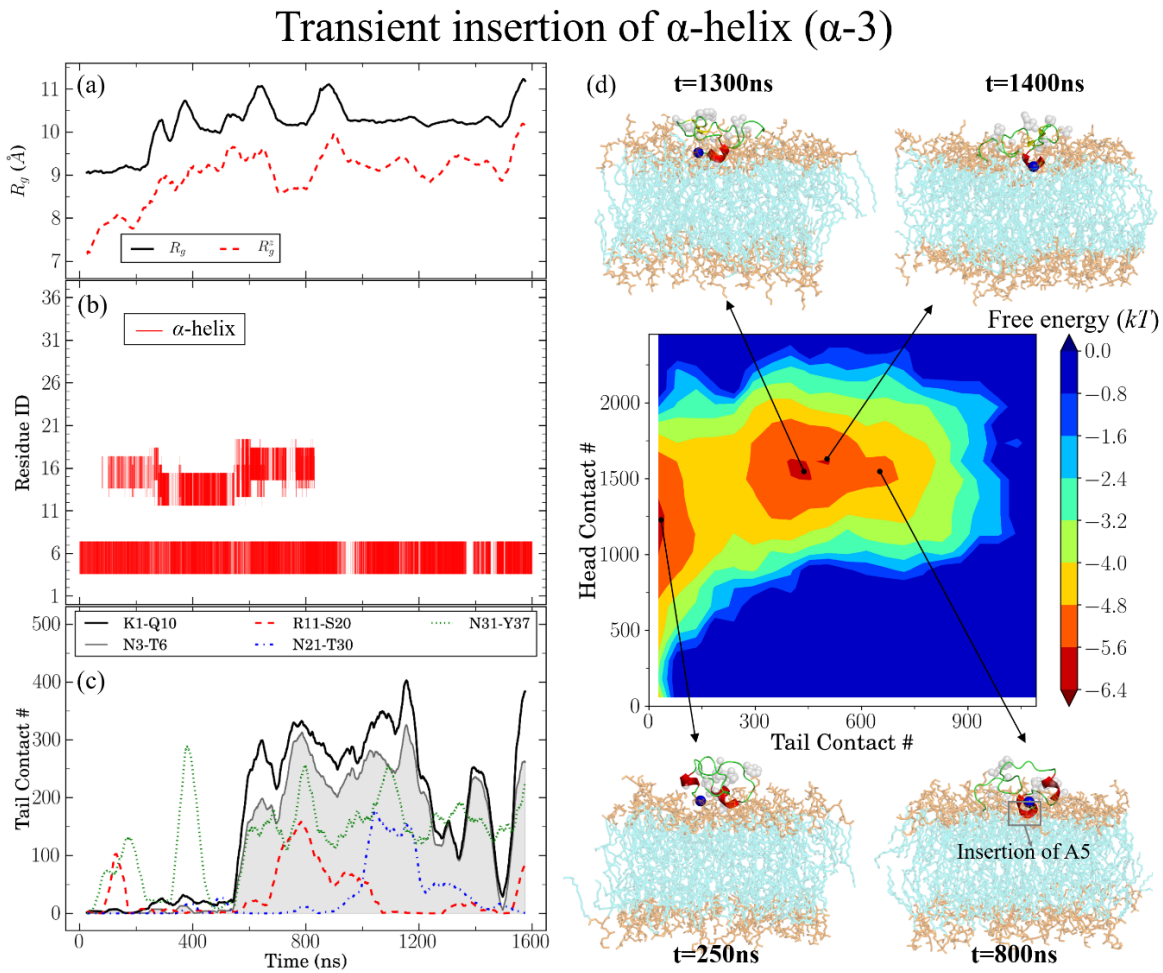

Fig. S3. Conformational dynamics of hIAPP transient α-helix formation upon binding to POPG membrane (labelled as α-3). (a) Time evolution of hIAPP radius of gyration about the principal axis R_g (black line) and z-axis R_g^z (red line). (b) Time evolution of α-helix secondary structure. (c) Time evolution of contact number between hIAPP segments and lipid tail groups: segment K1-Q10 (black line); segment N3-T6 (light black line); segment R11-S20 (red line); segment N21-T30 (blue line); segment N31-Y37 (green line). The segment N3-T6 is responsible for the N-terminal insertion into the lipid tail groups. The lines in (a) and (c) were smoothed via a 50-ns sliding window. (d) Free energy landscape is projected onto hIAPP contact number with lipid tail groups (x-axis) and head groups (y-axis), indicating the hIAPP insertion depth. Representative conformations of free energy minima are shown around with arrows directed. The conformation representation is the same as that in Fig. S2(d).

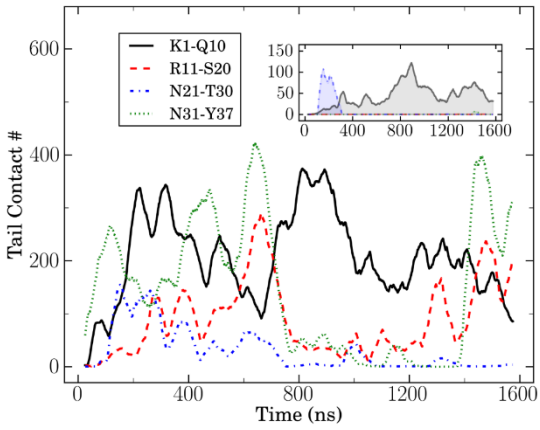

Fig. S4. Time evolution of contact numbers between hIAPP segments and POPG tail groups in the β-sheet hIAPP trajectory shown in main-text Fig. 4: segment K1-Q10 (black line); segment R11-S20 (red line); segment N21-T30 (blue line); segment N31-Y37 (green line). Inset is the contact number of hydrophobic residues in each segment. Among the hydrophobic residues, only residues A5A8 (gray line) and F23 (blue line) have a few contacts with lipid tail groups. The lines were smoothed via a 50-ns sliding window.

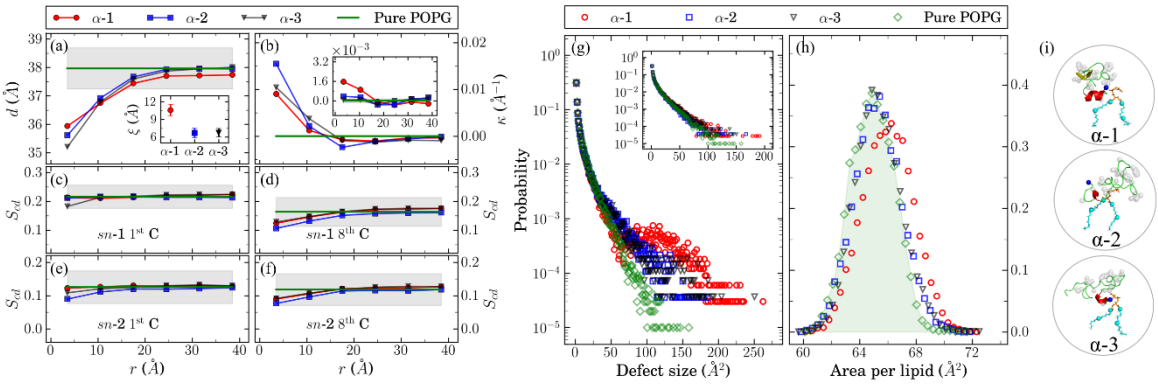

Fig. S5. Membrane deformation induced by α-helical hIAPP monomers. Each plot contains the results of α-helical hIAPP inserting into membrane in main-text Fig. 3 (α-1: red circles), and α-helical hIAPP on membrane surface in Fig. S2 (α-2: blue squares), and α-helical hIAPP on membrane surface in Fig. S3 (α-3: black triangles), in comparison with that of pure POPG bilayer (green line with gray-shaded area for the standard deviation in (a-f), and green diamonds in (g, h)). (a-f) Membrane structural change as a function of the lateral radial distance r to the position of minimal membrane thickness. (a) Membrane thickness d. The inset plots the coherence length ξ of the thickness deformation fitting by Eq. (1). (b) Membrane curvature κ of the hIAPP-bound leaflet. The inset plots the κ of hIAPP-free leaflet. (c-f) Membrane tail order parameter S_{cd} of the hIAPP-bound leaflet. (c) S_{cd} of 1st carbon atom in chain *sn*-1. (d) S_{cd} of 8th carbon atom in chain *sn*-1. (e) S_{cd} of 1st carbon atom in chain *sn*-2. (f) S_{cd} of 8th atom in chain *sn*-2. (g) The size distribution of the hydrophobic defects in the hIAPP-bound membrane leaflets. The inset plots the distribution in the hIAPP-free membrane leaflets. (h) The probability distribution of area per lipid (APL). (i) Representative hIAPP conformations and the closest POPG lipid molecules. The conformation representation is the same as Fig. S2(d). The 1st and 8th carbon atoms in the tail chains are shown in cyan spheres.

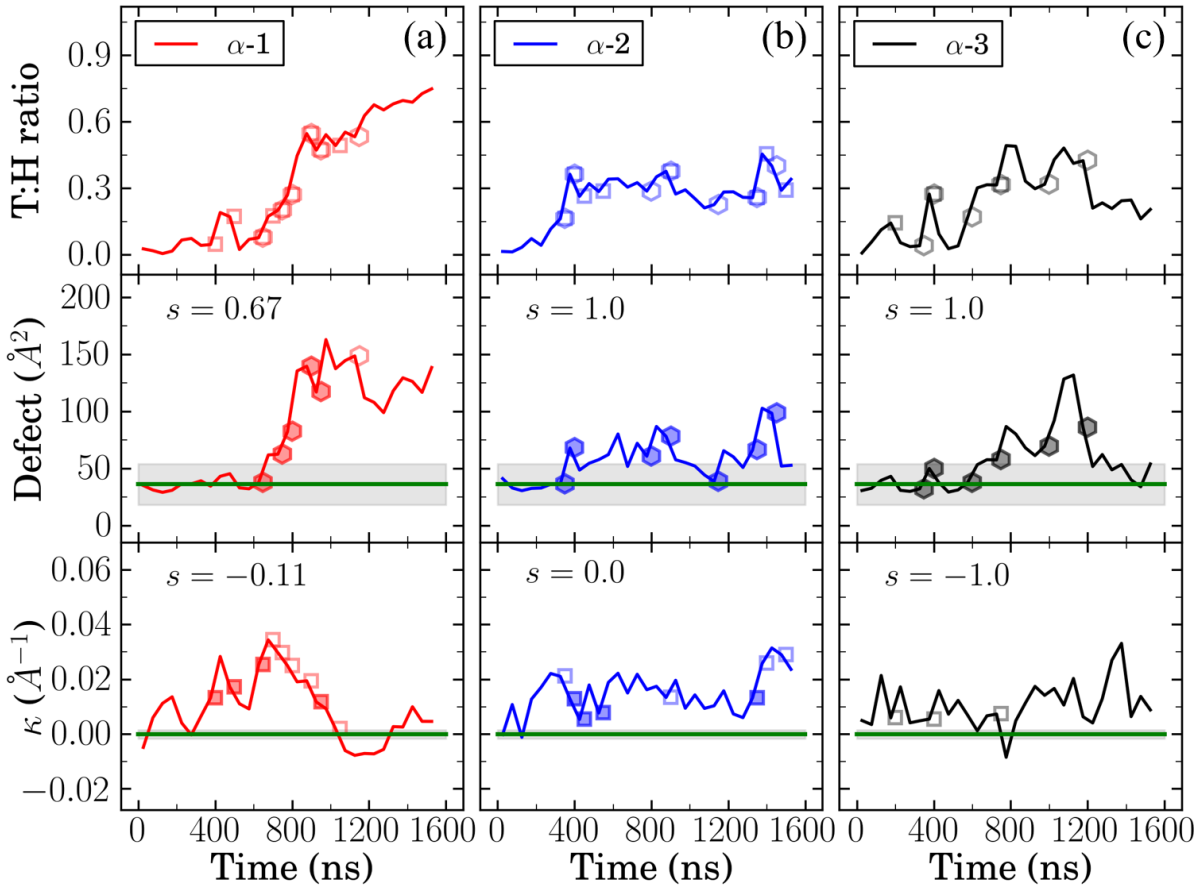

Fig. S6. Synchronization between α-helical hIAPP insertion and membrane deformation. In each plot, the top panel is the time evolution of ratio of the hIAPP-tail contact number to the hIAPP-head contact number (T:H ratio), the middle one is the size of the largest membrane hydrophobic defects, and the bottom one is the mean curvature κ around the position of minimal membrane thickness. The synchronization factors s of T:H ratio with defect size and curvature κ are calculated for hexagon and square points respectively, which correspond to the large changes. The filled or empty symbols indicate positive or negative correlation, respectively. (a) The α-helical hIAPP inserting into membrane (α-1), the same as the main-text Fig. 6(b). (b) The α-helical hIAPP on membrane surface in Fig. S2 (α-2). (c) The α-helical hIAPP on membrane surface in Fig. S3 (α-3). The green lines plot the average values of pure POPG bilayer without hIAPP, with gray shaded area for the standard deviation.

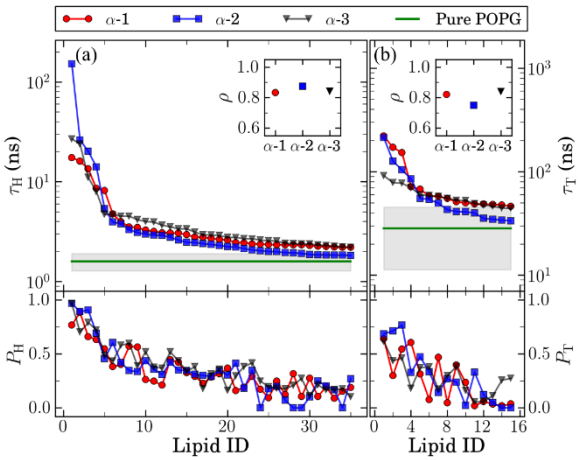

Fig. S7. Slow-down of lipid rotations induced by α-helical hIAPP binding. Each plot shows the results of α-1 (red circles), α-2 (blue squares) and α-3 (black triangles) hIAPP, in comparison with that of pure POPG bilayer (green line, with gray-shaded area for the standard deviation). (a) The head group rotational relaxation time-scales τ_H and contact probabilities P_H with hIAPP. The top panel is rotational relaxation time-scales τ_H of head group. The bottom panel is the contact probabilities P_H of lipid head groups with hIAPP, sorted in the descending order of τ_H. The inset is the Spearman's rank correlation coefficient ρ between τ_H and P_H. (b) The tail group rotational relaxation time-scales τ_T and contact probabilities P_T with hIAPP. The top panel is rotational relaxation time-scales of tail group τ_T. The bottom panel is the contact probabilities P_T of lipid tail groups with hIAPP, sorted in the descending order of τ_T. The inset is the Spearman's rank correlation coefficient ρ between τ_T and P_T.

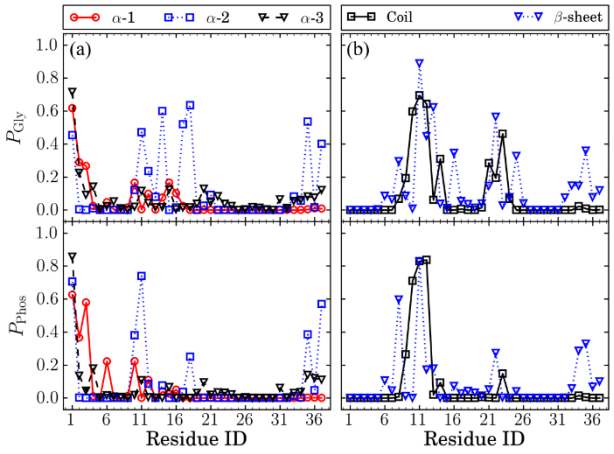

Fig. S8. Residue-based contact probability P of hIAPP with the lipid whose rotational relaxation time of head group τ_H is the slowest. The top panels are the P between hIAPP and lipid glycerol groups, and the bottom ones are the P between hIAPP and lipid phosphate groups. (a) The P in α-helical-rich trajectories: the α-1 trajectory (red circles), the α-2 trajectory (blue squares), and the α-3 trajectory (black triangles). (b) The P in the coil (black squares) and β-sheet (blue triangles) trajectories.

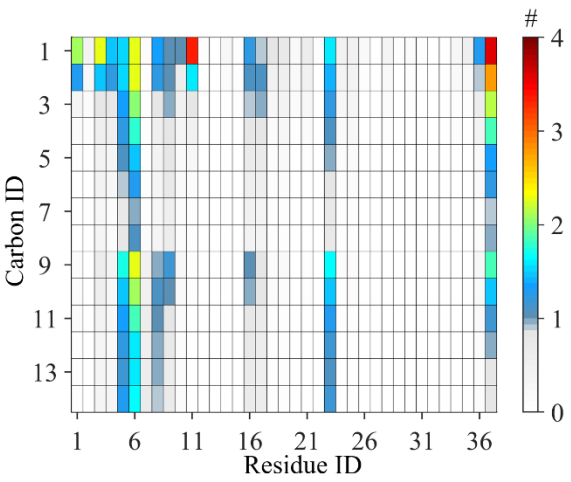

Fig. S9. Average contact number of each hIAPP residue with each hydrocarbon group in tail groups. The *x*-axis is the hIAPP residue ID. The *y*-axis is ID of carbon ID in lipid tail groups, starting from the 1st carbon atom closest to the lipid head groups, to 14th one near the lipid ends. The average contact number between hIAPP residue and POPG tail hydrocarbon is color-coded according to the color bar shown on the right.

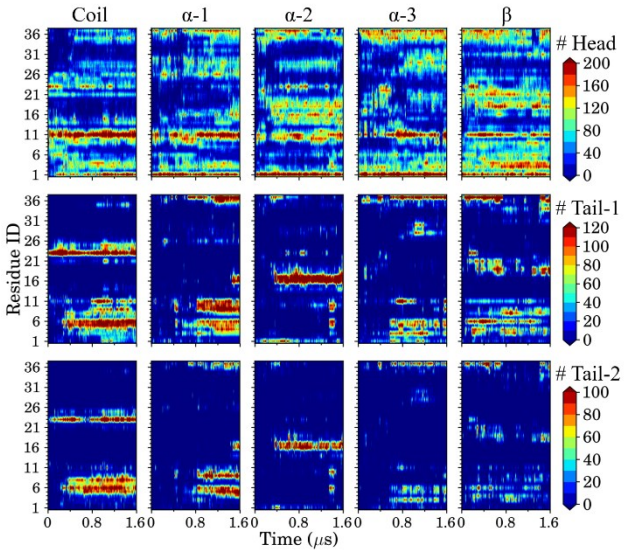

Fig. S10. Time evolution of number of contacts of each hIAPP residue with POPG head groups (top row), with POPG tail segments Tail-1 from the 1st carbon to the 7th carbon (middle row), and with POPG tail segments Tail-2 from the 8th carbon to the end (bottom row).

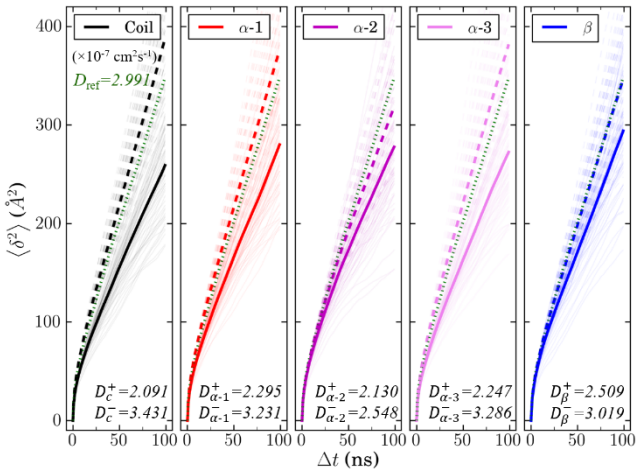

Fig. S11. Time-averaged mean square displacements (MSD) $\langle \delta^2 \rangle$ of hIAPP-bound POPG leaflet (solid lines) and those of hIAPP-free leaflet (dashed lines), in comparison with the MSD of pure POPG bilayer (green dotted lines). In each panel, the thick lines represent the average MSD of all lipids in the leaflet, and the thin lines represent those of individual lipid molecules. The diffusion coefficient D^+ of hIAPP-bound leaflet, D^- of hIAPP-free leaflet, and D^{ref} of pure POPG bilayer are labelled.

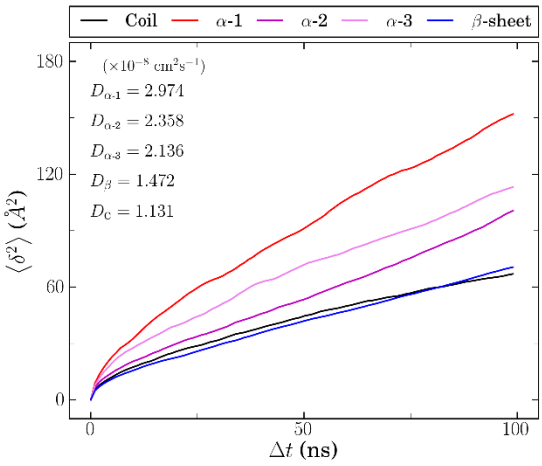

Fig. S12. Time-averaged MSD $\langle \delta^2 \rangle$ of hIAPP, with the center of mass of POPG leaflet bound with hIAPP as the reference: α-1 trajectory (red line); α-2 trajectory (purple line); α-3 trajectory (pink line); β-sheet trajectory (blue line); coil trajectory (black line). The hIAPP diffusion coefficients *D* are labelled.